Eur. Phys. J. C (2026) 86:402
https://doi.org/10.1140/epjc/s10052-026-15704-1

THE EUROPEAN PHYSICAL JOURNAL C

Regular Article - Theoretical Physics

Two-throat asymptotically flat wormholes

Mauricio Cataldo[2,1,a], **Antonella Cid**[1,2,b], **Pedro Labraña**[1,2,c]

[1] Departamento de Física, Universidad del Bío-Bío, Casilla 5-C, Concepción, Chile
[2] Centro de Ciencias Exactas, Universidad del Bío-Bío, Casilla 447, Chillán, Chile

Received: 1 January 2026 / Accepted: 7 April 2026

Abstract We present a systematic construction of traversable wormhole spacetimes featuring two symmetric throats within the framework of General Relativity. Our approach employs the embedding formalism by imposing the analytic relation $r - r_0 = K(z^2 - a)^2$ between the radial coordinate and the embedding function, which naturally guarantees the flare-out condition at both throats. This ansatz yields a composite shape function $b(r)$ consisting of two branches: an asymptotically flat branch ($\epsilon = +1$) extending to spatial infinity, and an intermediate tunnel branch ($\epsilon = -1$) with restricted domain $r_0 \leq r \leq r_0 + Ka^2$, connecting the two throats positioned at $z = \pm\sqrt{a}$ with separation $2\sqrt{a}$. Analysis of the Einstein field equations reveals that the supporting matter violates the weak, null, and dominant energy conditions throughout the spacetime, while the strong energy condition is identically satisfied with $\rho + p_r + 2p_t = 0$. A critical finding is the direct connection between throat separation and energy density: configurations with $0 < a < 1/(16Kr_0)$ admit positive energy density at the throats with phantom-type radial pressure ($\omega_r < -1$) and dark-energy-like effective behavior ($\omega_{\text{eff}} < 0$), whereas larger separations $a > 1/(16Kr_0)$ require negative energy density. Notably, configurations with phantom matter at the throats require such small values of a that the intermediate tunnel region becomes almost imperceptible, with the two throats nearly coincident, approaching the limiting case of a single-throat geometry. The geometric structure is visualized through embedding diagrams, which demonstrate that increasing the parameter a produces more pronounced and sharply defined throats. This work establishes that multi-throat wormhole geometries can be systematically generated through embedding techniques, providing a complementary approach to field-theoretic constructions and revealing how topological complexity relates to exotic matter distributions in traversable spacetimes.

1 Introduction

In classical general relativity the Einstein field equations admit a remarkable class of static solutions that describe spacetime tunnels connecting either two distant regions of our Universe or even separate universes. These geometrical configurations, known as wormholes, exhibit spacetime that may be either flat or curved in regions far from the tunnel. The Morris and Thorne (M–T) wormhole ansatz was originally formulated for static, spherically symmetric metrics in the form [1,2]

$$ds^2 = -e^{2\phi(r)}dt^2 + \frac{dr^2}{1 - \frac{b(r)}{r}} + r^2(d\theta^2 + \sin^2\theta d\varphi^2), \quad (1)$$

where $e^{2\phi(r)}$ and $b(r)$ are arbitrary functions of the radial coordinate r, known as redshift function and shape function, respectively.

For a viable wormhole geometry, these two functions must satisfy some general constraints discussed in Refs. [1,2]. These constraints establish the minimum conditions to produce a geometry with two regions connected by a bridge, namely:

- Constraint 1: The no-horizon condition requires that $e^{\phi(r)}$ remains finite throughout the spacetime to ensure the absence of event horizons and singularities.
- Constraint 2: The throat condition specifies that at the minimum radius r_0, the shape function satisfies

$$b(r) = r_0. \quad (2)$$

- Constraint 3: Morris and Thorne established that to maintain the structure of a traversable wormhole, a fundamen-

[a] e-mail: mcataldo@ubiobio.cl (corresponding author)
[b] e-mail: acidm@ubiobio.cl
[c] e-mail: plabrana@ubiobio.cl

Published online: 22 April 2026

tal geometric condition known as the flare-out condition must be satisfied, which guarantees a minimum size and ensures that spacetime opens toward both sides of the throat. This geometric condition is expressed as:

$$\frac{d^2r}{dz^2} > 0, \tag{3}$$

where the variable z is defined as:

$$\frac{dz}{dr} = \pm\left(\frac{b(r)}{r-b(r)}\right)^{1/2}, \tag{4}$$

where the function $z(r)$ is known in the literature as the embedding function and plays a fundamental role in the geometric visualization of a wormhole. The flare-out condition may also be written as:

$$\frac{b(r)-rb'(r)}{2b^2(r)} > 0. \tag{5}$$

- Constraint 4: Asymptotic flatness condition, i.e. as $l \to \pm\infty$ (or equivalently, $r \to \infty$)

$$\frac{b(r)}{r} \to 0. \tag{6}$$

Although asymptotically flat wormhole geometries are of particular interest, more general wormhole spacetimes have been studied in the literature [3–5].

- Constraint 5: Finiteness of the proper radial distance, i.e.

$$\frac{b(r)}{r} \leq 1, \tag{7}$$

(for $r \geq r_0$) throughout the spacetime. The equality holds only at the throat. Equation (7) is required in order to ensure the finiteness of the proper radial distance $l(r)$ defined by

$$l(r) = \pm\int_{r_0}^{r} \frac{dr}{\sqrt{1-\frac{b(r)}{r}}}, \tag{8}$$

where the $\pm$ signs refer to the two asymptotically flat regions connected by the wormhole. Note that the condition (7) assures that the metric component g_{rr} in Eq. (1) does not change sign for any $r \geq r_0$.

Wormholes are supported by exotic matter sources that typically violate all classical energy conditions [6]. These conditions are physically motivated constraints imposed on the energy–momentum tensor, intended to capture fundamental properties expected of the matter content in a given spacetime. For anisotropic matter sustaining a traversable wormhole, the energy–momentum tensor takes the form $T^{\mu}_{\nu} = \mathrm{diag}(-\rho, p_r, p_t, p_t)$. The energy conditions are formulated in terms of the following inequalities [6]:

1. Weak Energy Condition (WEC):

   $\rho \geq 0$, $\rho + p_r \geq 0$ and $\rho + p_t \geq 0$.

2. Null Energy Condition (NEC):

   $\rho + p_r \geq 0$ and $\rho + p_t \geq 0$.

3. Dominant Energy Condition (DEC):

   $\rho \geq |p_r|$ and $\rho \geq |p_t|$, or equivalently $\rho + p_r \geq 0$, $\rho + p_t \geq 0$ and $\rho - p_r \geq 0$ and $\rho - p_t \geq 0$.

4. Strong Energy Condition (SEC):

   $\rho + p_r + 2p_t \geq 0$.

While the standard Morris–Thorne construction describes a wormhole with a *single* throat, nothing in the underlying field equations prevents more complex topological structures. Multi-throat geometries represent the natural next step in this hierarchy: they introduce an intermediate tunnel region bounded by two distinct throats, allow for different distributions of exotic matter across multiple junctions, and provide additional geometric parameters, most notably the throat separation, that control how matter content and energy condition violations scale with topological complexity. Such configurations may also offer novel mechanisms for minimizing the total amount of exotic matter required, since the exoticity can in principle be distributed across multiple throats rather than concentrated at a single junction. The two-throat case studied here is the simplest non-trivial extension of the standard geometry, enabling direct comparison with single-throat solutions and revealing how the presence of multiple throats fundamentally alters the geometric and physical properties of traversable wormholes. Despite this motivation, the systematic construction of asymptotically flat two-throat wormholes within the Morris–Thorne framework using purely geometric methods that guarantee the flare-out condition by construction remains an open problem in the literature.

From a broader theoretical and phenomenological perspective, two-throat wormhole geometries are relevant for several reasons. First, multi-throat geometries generically produce richer geodesic structures than single-throat wormholes, potentially leaving observable imprints in gravitational lensing and shadow morphology that could distinguish them from both black holes and standard single-throat wormholes [7,8]. Second, the distribution of exotic matter across two throats rather than a single junction raises the question of whether multi-throat configurations can be supported by smaller total amounts of energy-condition-violating matter than their single-throat counterparts, a question with direct

bearing on the physical plausibility of traversable wormholes [6]. Third, the present work demonstrates that the matter supporting two-throat geometries can exhibit phantom-type behavior with positive energy density, a configuration consistent with dark energy models not ruled out by current cosmological observations [9–11], thereby connecting multi-throat wormhole physics to broader questions in cosmology and gravitational theory.

The present work addresses this gap with three specific objectives. The first is to construct an explicit closed-form family of asymptotically flat two-throat traversable wormhole solutions by extending the embedding formalism of Ref. [12] to a quartic ansatz, with the flare-out condition satisfied by construction at every throat. The second is to characterize completely the geometric and matter properties of these solutions, including junction conditions, curvature invariants, energy condition violations, and ADM mass. The third is to determine whether the throat separation parameter provides explicit analytical control over the severity of the exotic matter requirements. Our working hypothesis is that the embedding approach does admit two-throat solutions, and that the throat separation parameter a governs not only the geometry but also the sign and magnitude of the energy density, establishing a direct link between topological scale and matter exoticity that has no counterpart in single-throat wormholes. The key physical insight of the present construction is precisely this link: by tuning the single geometric parameter a, one can continuously transition between a physically less extreme regime, supported by phantom-type matter with positive energy density, and a more exotic regime requiring negative energy density, revealing that topological complexity and matter exoticity are not independent but are instead governed by a common geometric scale.

Multi-throat wormhole geometries have been studied through several distinct field-theoretic approaches. Rodrigues and Silva [7,13] identified multiple throats and anti-throats in black-bounce spacetimes constructed by coupling phantom scalar fields to nonlinear electrodynamics (NED): in their framework, the metric function $\Sigma(r)$ is postulated and the field sources are then determined from the Einstein equations, with throats and anti-throats identified *a posteriori* as minima and maxima of the areal function. The resulting geometries generically interpolate between regular black holes and wormholes depending on the parameter values, and therefore include configurations with horizons. Crispim et al. [8] extended this analysis to the same class of $\Sigma(r)$ geometries, determining explicitly the phantom scalar field and NED sources compatible with the field equations and showing that distinct scalar field profiles (arctangent and hyperbolic tangent) generate the same spacetime geometry, while demonstrating that energy conditions can be partially satisfied in certain regions. By contrast, the present work constructs asymptotically flat traversable wormhole spacetimes with two symmetric throats by imposing the flare-out condition by construction through the embedding ansatz (9), which guarantees traversability throughout the parameter space without reference to a specific field theory. The throat separation enters as an explicit geometric parameter a that directly controls the sign and magnitude of the energy density at the throats, establishing an analytical link between topological scale and matter exoticity that is not available in the $\Sigma(r)$-based approach.

The novelty of the present construction is threefold. First, whereas existing multi-throat solutions are obtained by postulating a metric function and identifying throats *a posteriori* through extrema of the areal function [7,8,13], our embedding ansatz imposes the flare-out condition *by construction* at every throat, guaranteeing traversability throughout the entire parameter space without reference to a specific field-theoretic source. Second, the ansatz yields closed-form analytical expressions for the shape function, the energy density, and all pressure components, enabling exact rather than numerical analysis of the geometric and matter properties. Third, and most significantly, the throat separation enters as an explicit geometric parameter that controls analytically the sign and magnitude of the energy density at the throats: this direct link between topological scale and matter exoticity has no counterpart in field-theoretic constructions, where the matter distribution is determined implicitly by the choice of field source rather than by a geometric parameter with transparent physical meaning

In this work, our main goal is to construct a family of traversable wormhole solutions with two throats by employing the embedding condition (4), which arises from embedding a spacelike slice defined by $t = \text{const}$ and $\theta = \pi/2$ of the metric (1) into Euclidean space in cylindrical coordinates. This geometric approach was previously used in Ref. [12] to construct a static traversable wormhole, with its geodesic structure subsequently analyzed in Ref. [14]. This method guarantees the fulfillment of the flare-out condition and enables us to determine the shape function $b(r)$ that satisfies the criteria necessary for describing traversable wormholes.

This paper is organized as follows: in Sect. 2, we briefly outline the key aspects of the geometric approach used to construct the shape function $b(r)$ through the embedding formalism. Section 3 focuses on the wormhole metric, the Einstein field equations, and the analysis of energy conditions. In Sect. 4, we analyse the geometric structure of the two-throat configuration and present the embedding diagrams for different parameter regimes, considering both configurations with positive and negative energy densities. Finally, our conclusions are presented in Sect. 5.

2 The approach to construct the shape function $b(r)$

To construct the wormhole, we employ the embedding equation (4) by imposing an analytic expression for the embedding function $z(r)$ to subsequently determine the analytic form of the shape function. From Eq. (4) we conclude that it defines a dependence between the variable z and the radial coordinate r. Accordingly, in this work we postulate such a dependence that both the function $z(r)$ and its inverse $r(z)$ have analytical form.

Our ansatz for constructing the traversable wormhole is given by

$$r - r_0 = K\left(z^2 - a\right)^2. \tag{9}$$

Here, r_0 is a constant with dimensions of length L, while a is a real constant with dimensions of L^2. The parameter $K > 0$ has dimensions of L^{-3}, and the coordinate z carries dimensions of length L.

Note that the first and second derivatives are given by:

$$\frac{dr}{dz} = 4Kz(z^2 - a), \frac{d^2r}{dz^2} = 4K(3z^2 - a), \tag{10}$$

respectively.

The relation (9) also allows us to express z as a function of the radial coordinate r. In this case, the function $z(r)$ is multivalued and takes the form:

$$z_1(r) = +\sqrt{a + \sqrt{\frac{r - r_0}{K}}}, \tag{11}$$

$$z_2(r) = +\sqrt{a - \sqrt{\frac{r - r_0}{K}}}, \tag{12}$$

$$z_3(r) = -\sqrt{a - \sqrt{\frac{r - r_0}{K}}}, \tag{13}$$

$$z_4(r) = -\sqrt{a + \sqrt{\frac{r - r_0}{K}}}. \tag{14}$$

It is evident from Eqs. (11)–(14) that, for the expressions $z_i(r)$, with $i = 1, 2, 3, 4$, to be real-valued, the basic condition $r \geq r_0$ must be satisfied.

To unify the four branches of the embedding function, we write it compactly in the following form:

$$z(r) = \pm\sqrt{a + \epsilon\sqrt{\frac{r - r_0}{K}}}, \tag{15}$$

where $\epsilon = \pm 1$. We then obtain for its first derivative:

$$\frac{dz}{dr} = \pm\frac{1}{4K\sqrt{\frac{r-r_0}{K}}\sqrt{a + \epsilon\sqrt{\frac{r-r_0}{K}}}}, \tag{16}$$

and by substituting this expression into Eq. (4), we obtain for the shape function:

$$b(r) = \frac{r}{16K(r - r_0)\left(a + \epsilon\sqrt{\frac{r-r_0}{K}}\right) + 1}. \tag{17}$$

Notice that, in general, from Eq. (16) we obtain that at $r = r_0$ the slope of $z(r)$ becomes infinite, as we should expect in the case of a wormhole. However, it should be noted that the first derivative of the embedding function (16) also becomes infinite at

$$r = Ka^2 + r_0, \tag{18}$$

and therefore we must elucidate the location of the wormhole throat.

It should be emphasized that the divergence of dz/dr at $r = Ka^2 + r_0$ has a fundamentally different physical interpretation than the divergence at the throat $r = r_0$. While the latter corresponds to the wormhole throat where $b(r_0) = r_0$ and represents a minimum in the radial coordinate, the former marks the upper boundary of the intermediate tunnel connecting the two throats. At this radius, both embedding functions $z_2(r)$ and $z_3(r)$ vanish, and the metric component g^-_{rr} changes sign for $r > Ka^2 + r_0$, restricting the $\epsilon = -1$ branch to the domain $r_0 \leq r \leq r_0 + Ka^2$, while the $\epsilon = 1$ branch extends asymptotically to infinity.

It is evident that the shape function (17) satisfies the condition (2) for $r = r_0$, so the throat of the wormhole is located at r_0. For the flare-out condition, Eq. (5) leads to

$$12\epsilon\sqrt{r - r_0} + 8\sqrt{K}a > 0. \tag{19}$$

This same inequality is recovered by substituting Eq. (15) into the second expression of Eq. (10). The condition (19) implies that $a > 0$ at the throat, hence, only positive values of the parameter a are allowed to fulfill the flare-out condition.

Equation (15) is directly related to the location of the wormhole throat. Evaluating this function at the throat yields:

$$z(r_0) = \epsilon\sqrt{a}. \tag{20}$$

Since the flare-out condition requires $a > 0$, we conclude that there exist wormhole configurations featuring two symmetric throats located at $+\sqrt{a}$ and $-\sqrt{a}$. This configuration, consists of two tunnels connected through an intermediate region. Consequently, each throat must independently satisfy the flare-out condition, as both throats open outward toward their respective asymptotic regions.

3 The wormhole metric, the field equations and energy conditions

From Eqs. (1) and (17) the wormhole metric takes the following form:

$$ds^2 = -e^{2\phi(r)}dt^2 + \frac{dr^2}{1-\frac{1}{16K(r-r_0)\left(a+\epsilon\sqrt{\frac{r-r_0}{K}}\right)+1}} + r^2\left(d\theta^2+\sin^2\theta d\varphi^2\right), \tag{21}$$

and the field equations are given by:

$$\kappa\rho(r) = \frac{-8\sqrt{K}\epsilon\,(r+2r_0)\sqrt{r-r_0}-16Kar_0+1}{\left(16(r-r_0)\left(Ka+\sqrt{K}\epsilon\sqrt{r-r_0}\right)+1\right)^2 r^2}, \tag{22}$$

$$\kappa p_r(r) = 2\left(1-\frac{1}{16K(r-r_0)\left(a+\epsilon\sqrt{\frac{r-r_0}{K}}\right)+1}\right)\frac{\phi'(r)}{r} - \frac{1}{\left(16K(r-r_0)\left(a+\epsilon\sqrt{\frac{r-r_0}{K}}\right)+1\right)r^2}, \tag{23}$$

$$\kappa p_t(r) = \left(1-\frac{1}{16K(r-r_0)\left(a+\epsilon\sqrt{\frac{r-r_0}{K}}\right)+1}\right)\left[\phi''(r)+\phi'^2(r)+\frac{\phi'(r)}{r}\right] + \left(\phi'(r)+\frac{1}{r}\right)\left[\frac{4\left(3\epsilon\sqrt{K(r-r_0)}+2Ka\right)}{\left(16K(r-r_0)\left(a+\epsilon\sqrt{\frac{r-r_0}{K}}\right)+1\right)^2}\right], \tag{24}$$

where the prime denotes the derivative d/dr and $\kappa = 8\pi G$.

To analyse the physical viability of this wormhole configuration, it is necessary to examine if the energy conditions are satisfied or violated by the matter content. It is well known that the flare-out condition (5), which at the wormhole throat takes the form $b'(r_0) < 1$, leads to the violation of classical energy conditions.

We begin by evaluating the energy density, as well as the radial and tangential pressures, at the throats. From Eqs. (22)–(24) we obtain

$$\kappa\rho(r_0) = \frac{1-16Kar_0}{r_0^2}, \tag{25}$$

$$\kappa p_r(r_0) = -\frac{1}{r_0^2}, \tag{26}$$

$$\kappa p_t(r_0) = 8Ka\left(\phi'(r_0)+\frac{1}{r_0}\right). \tag{27}$$

It is important to note that equations (22)–(24) show that the relations (25)-(27) hold independently of the branch considered, i.e., for $\epsilon = 1$ and $\epsilon = -1$.

Accordingly, the relevant combinations appearing in the energy conditions take following form:

$$\rho(r_0)+p_r(r_0) = -\frac{16Ka}{\kappa r_0}, \tag{28}$$

$$\rho(r_0)+p_t(r_0) = \frac{1-8Kar_0}{\kappa r_0^2}+\frac{8Ka\phi'(r_0)}{\kappa}, \tag{29}$$

$$\rho(r_0)-p_r(r_0) = \frac{2(1-8Kar_0)}{\kappa r_0^2}, \tag{30}$$

$$\rho(r_0)-p_t(r_0) = \frac{1-24Kar_0}{\kappa r_0^2}-\frac{8Ka\phi'(r_0)}{\kappa}, \tag{31}$$

$$\rho(r_0)+p_r(r_0)+2p_t(r_0) = \frac{16Ka\phi'(r_0)}{\kappa}. \tag{32}$$

We begin the analysis of the energy conditions with the WEC. From Eq. (25), we find that $\rho(r_0) \geq 0$ if

$$0 < a \leq \frac{1}{16Kr_0}, \tag{33}$$

and $\rho(r_0) \leq 0$ if

$$a \geq \frac{1}{16Kr_0}. \tag{34}$$

Therefore, it is possible to construct wormhole configurations in which the energy density is positive.

On the other hand, from Eq. (28) we observe that for positive values of the parameter a the combination $\rho(r_0)+p_r(r_0)$ is always negative. Additionally, the condition (29) is non-negative only if $\frac{1-8Kar_0}{r_0^2}+8Ka\phi'(r_0) \geq 0$. For a wormhole configuration free of tidal forces, i.e., setting $\phi(r) = 0$, the condition (29) is satisfied for $0 < a \leq \frac{1}{8Kr_0}$ and violated for $a > \frac{1}{8Kr_0}$. In conclusion, the WEC is violated by the matter supporting the two-throats wormhole configuration.

In this way, the fact that Eq. (28) yields $\rho(r_0)+p_r(r_0) < 0$ for any $a > 0$ indicates that the WEC, NEC, and DEC are violated, whereas only the SEC may hold if $\phi'(r_0) \geq 0$. This, in turn, implies that for the SEC to be satisfied, the function $e^{2\phi(r)}$ must be monotonically increasing (non-decreasing). For asymptotically flat wormholes, we can require that $\phi(r) \to 0$ as $r \to \infty$ (although $\phi(r) \to$ constant would suffice after a time coordinate rescaling), and that $\phi'(r_0) > 0$ with $\phi'(r) \to 0$ at spatial infinity.

Additionally, note that these wormholes can be supported by phantom matter. Indeed, from Eqs. (25)–(27) one can define directional equations of state parameters as follows:

$$\omega_r = \frac{p_r}{\rho} = -\frac{1}{1-16Kar_0}, \tag{35}$$

$$\omega_t = \frac{p_t}{\rho} = \frac{8Kar_0(1+r_0\phi'(r_0))}{1-16Kar_0}. \tag{36}$$

It is of interest to consider the interval (33). If the parameter satisfies $0 < a < \frac{1}{16Kr_0}$, then the energy density is positive, and the equations of state yield $\omega_r < -1$ and $\omega_t > 0$ for $\phi'(r_0) > 0$. This implies that the matter supporting the wormhole is of phantom type. For $a = \frac{1}{16Kr_0}$, we have $\rho(r_0) = 0$, and the state parameters diverge: $\omega_r \to -\infty$, $\omega_t \to \infty$.

We now clarify why the regime $0 < a < 1/(16Kr_0)$, in which $\rho(r_0) > 0$, is physically distinguished from the regime $a > 1/(16Kr_0)$, where $\rho(r_0) < 0$. As noted above, the null energy condition (NEC) is violated in both cases, since $\rho(r_0) + p_r(r_0) = -16Ka/(\kappa r_0) < 0$ for all $a > 0$. The distinction is therefore not one of NEC compliance, but rather one of the *hierarchy* of energy condition violations and of observational plausibility.

When $\rho(r_0) > 0$, the matter at the throat satisfies the first requirement of the weak energy condition (WEC), namely $\rho \geq 0$, while violating only its second component $\rho + p_r \geq 0$. By contrast, when $\rho(r_0) < 0$ all components of the WEC are violated, including $\rho \geq 0$ itself, which represents the most severe form of energy condition violation admitted in classical field theory. The $\rho > 0$ regime therefore involves a strictly weaker and more constrained set of violations.

From an observational standpoint, matter with $\rho > 0$ and $\omega_r < -1$ is consistent with the class of phantom dark energy models [9,10], which are not ruled out by current cosmological observations. As emphasized by Lobo [11], phantom energy possesses precisely the two properties required to sustain traversable wormholes: a positive energy density, $\rho > 0$, and a violation of the null energy condition, $\rho + p < 0$. This makes it a physically motivated, if exotic, candidate for wormhole matter, and it has been widely studied as a natural source for these geometries [11]. Moreover, Lobo showed that traversable wormholes supported by phantom energy can in principle be constructed with arbitrarily small amounts of averaged null energy condition violating matter, further distinguishing this regime from configurations with $\rho < 0$, which require more severe violations of all classical energy conditions. Negative energy density, on the other hand, has no classical analog and lies entirely outside the domain of known physical fields. We therefore do not claim that the $\rho > 0$ regime is *stable*, a stability analysis lies beyond the scope of this work, but rather that it is physically less extreme, in the precise sense that it requires a strictly smaller departure from the classical energy conditions than the $\rho < 0$ regime.

We can also analyse the effective equation of state parameter, defined as $\omega_{\text{eff}} = \frac{p_r + 2p_t}{3\rho}$. Evaluating this at the throat, we obtain

$$\omega_{\text{eff}} = -\frac{1}{3} + \frac{16Kar_0^2\phi'(r_0)}{3(1 - 16Kar_0)}. \tag{37}$$

This expression reveals a critical value at $a = \frac{1}{16Kr_0}$. For $0 < a < \frac{1}{16Kr_0}$ with $\phi'(r_0) > 0$, we obtain $\omega_{\text{eff}} > -\frac{1}{3}$, corresponding to ordinary (non-exotic) matter. This result indicates that, when the matter content is described by its effective (isotropically averaged) equation of state, all standard energy conditions (WEC, NEC, DEC, and SEC) are satisfied in the effective sense. Conversely, for $a > \frac{1}{16Kr_0}$ with $\phi'(r_0) > 0$, we obtain $\omega_{\text{eff}} < -\frac{1}{3}$, indicating exotic matter with phantom-like or dark energy-like behavior. The limiting case $\omega_{\text{eff}} = -1/3$, achieved when $\phi'(r_0) = 0$, corresponds to a domain wall equation of state, marking the critical boundary between ordinary and exotic matter regimes.

Note that from Eqs. (34)–(36), we obtain $\omega_r \geq 0$ and $\omega_t \leq 0$ for $\phi'(r_0) > 0$.

In summary, the matter required to support this two-throat wormhole necessarily violates energy conditions.

The anisotropic fluid supporting the two-throat wormhole is obtained here via the inverse problem approach: the geometry is specified through the embedding ansatz (9), and the stress-energy tensor is then determined from the Einstein field equations (22)–(24). As such, no specific field theory is invoked, and the matter source is of a purely phenomenological nature. We can nonetheless examine whether the resulting $T_{\mu\nu}$ is structurally compatible with known field-theoretic sources.

A minimally coupled scalar field χ, whether normal ($\sigma = +1$) or phantom ($\sigma = -1$), with an arbitrary potential $V(\chi)$ always satisfies $p_t = -\rho$, independently of σ and V. This follows directly from the structure of the energy–momentum tensor, since $p_t = -\sigma X - V = -(\sigma X + V) = -\rho$, where $X = \frac{1}{2}(1 - b/r)(\chi')^2$. Our stress-energy tensor does not satisfy this relation in general: at the throat, $\kappa[p_t(r_0) + \rho(r_0)] = (1 - 8Kar_0)/r_0^2$, which vanishes only for the specific value $a = 1/(8Kr_0)$. A nonlinear electrodynamics (NLE) source with a purely radial magnetic field always imposes $\rho = p_r$, since $T^t{}_t = T^r{}_r$ for a magnetic configuration. This is also incompatible with our solution, where $\kappa[p_r(r_0) - \rho(r_0)] = 16Kar_0/r_0^2 \neq 0$. A radial electric NLE field, on the other hand, imposes $p_t = -\rho$, the same structural restriction as the scalar field, and is therefore equally incompatible.

These observations indicate that the $T_{\mu\nu}$ derived here does not correspond to any of these standard single-field sources. Candidate theories that are not ruled out on structural grounds include non-minimally coupled scalar fields ($\xi R\chi^2$), combinations of scalar and NLE fields, and effective stress-energy tensors arising in $f(R)$ gravity or Horndeski-type theories [7,8], all of which can produce genuinely anisotropic fluids with $p_r \neq p_t \neq \pm\rho$. The explicit identification of a field theory reproducing the exact stress-energy tensor $T_{\mu\nu}$ of this work is an interesting open problem that lies beyond its present scope.

It is worth emphasizing that the parameter a plays a crucial role in determining both the geometric structure and the

matter content of the two-throat wormhole. From a geometric perspective, this parameter controls the separation between the throats, which are located at $z = \pm\sqrt{a}$ in the embedding space, yielding a throat separation of $2\sqrt{a}$. Remarkably, this geometric parameter also directly determines the sign of the energy density at the throats. From Eqs. (33) and (34), we find that the energy density $\rho(r_0)$ at the throat changes from positive to negative values as a exceeds the critical value $a_c = \frac{1}{16Kr_0}$. It is important to note that the parameter K plays a complementary role: while it does not affect the throat locations $z = \pm\sqrt{a}$ directly, it modulates the critical threshold a_c through the inverse relation $a_c = \frac{1}{16Kr_0}$. Consequently, a larger value of K lowers a_c, restricting the range of throat separations $2\sqrt{a} < 2/\sqrt{16Kr_0}$ for which positive energy density is admissible, while a smaller K extends this range. In this sense, K acts as a scaling factor that controls how the geometric and matter content regimes are distributed in parameter space. Specifically, for throat separations corresponding to $0 < a < \frac{1}{16Kr_0}$, the wormhole is supported by positive energy density matter, whereas for larger separations with $a > \frac{1}{16Kr_0}$, negative energy density is required. This establishes a direct connection between the topological scale of the wormhole, quantified by the throat separation, and the nature of the exotic matter required to sustain it. Configurations with closely spaced throats (small a) can be supported by phantom-type matter with positive energy density but radial equation of state parameter $\omega_r < -1$, while more widely separated throats (large a) necessarily require matter with negative energy density. Moreover, since the critical separation scales as $2\sqrt{a_c} = \frac{1}{2\sqrt{Kr_0}}$, the geometric extent of the positive energy density regime depends sensitively on K: larger values of K restrict this regime to configurations with nearly coincident throats, while smaller values of K allow positive energy density over a wider range of throat separations. This relationship indicates that reducing the topological separation between the throats of a multi-throat wormhole may lead to configurations involving less severe violations of the classical energy conditions.

Figure 1 illustrates this behavior by displaying $\Delta z_c = \frac{1}{2\sqrt{Kr_0}}$ as a function of K. The curve separates two physically distinct regimes: configurations lying below it ($\Delta z < \Delta z_c$) are supported by matter with positive energy density, whereas those above it ($\Delta z > \Delta z_c$) necessarily require negative energy density. The monotonically decreasing character of Δz_c with K reveals that increasing the coupling parameter progressively restricts the positive energy density regime to wormhole geometries with nearly coincident throats. In the limit of large K, $\Delta z_c \to 0$, meaning that only configurations approaching the single-throat limit can be supported by matter with $\rho(r_0) > 0$. Conversely, for small K, the positive energy density regime extends over a wider range of throat separations, offering greater geometric freedom while maintaining the phantom-type matter content characterized by $\omega_r < -1$.

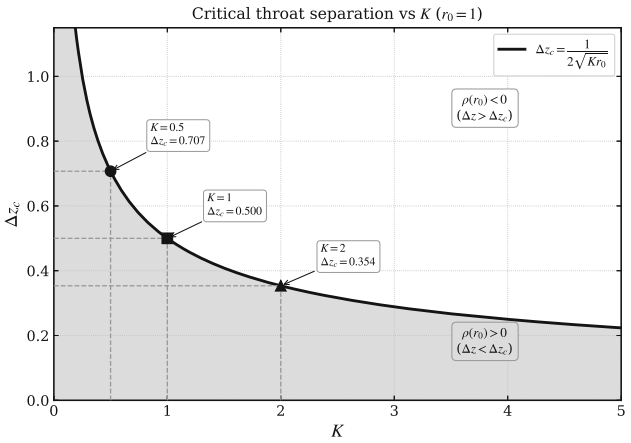

Fig. 1 Critical throat separation $\Delta z_c = \frac{1}{2\sqrt{Kr_0}}$ as a function of the parameter K, for $r_0 = 1$. The curve defines the boundary between two distinct matter regimes: configurations with throat separation $\Delta z < \Delta z_c$ (gray region) admit positive energy density $\rho(r_0) > 0$ at the throats, while configurations with $\Delta z > \Delta z_c$ (white region) necessarily require negative energy density $\rho(r_0) < 0$. Three representative values are marked: $K = 0.5$ ($\Delta z_c \approx 0.707$), $K = 1$ ($\Delta z_c = 0.500$), and $K = 2$ ($\Delta z_c \approx 0.354$). The monotonically decreasing behavior illustrates that larger values of K restrict the positive energy density regime to wormhole configurations with nearly coincident throats, while smaller values of K allow positive energy density over a wider range of throat separations

4 Geometric analysis and isometric embedding

In this section, we will examine several relevant aspects of the geometric structure of spacetime (21). To simplify our analysis, we set $\phi = 0$.

Note that the shape function $b(r)$ in Eq. (17) is a composite function describing the complete wormhole geometry through two branches: $b_+(r)$ (with $\epsilon = +1$) and $b_-(r)$ (with $\epsilon = -1$), denoted by $WH+$ and $WH-$ respectively. These branches join continuously at the throat location $r = r_0$ where $b_+(r_0) = b_-(r_0) = r_0$, ensuring a smooth geometric transition despite having infinite derivatives at this point, which is the expected behavior for wormhole throats with vertical tangents. Correspondingly, the ratio $b(r)/r$ in the metric (21) exhibits this two-branch structure, with both ratios satisfying $b_\pm(r_0)/r_0 = 1$ at the throats, causing the radial metric component g_{rr} to diverge and properly characterizing the two symmetric throats of the wormhole.

The first important observation is that these two branches exhibit different asymptotic behaviours and geometric domains. The $WH+$ branch is characterized by the shape function $b_+(r) = \frac{r}{16K(r-r_0)(a+\sqrt{\frac{r-r_0}{K}})+1}$, which makes this branch asymptotically flat, as the form of $b_+(r)$ ensures that con-

dition (6) is satisfied with $b_+(r)/r \to 0$ as $r \to \infty$. This conclusion is further supported by the Einstein field equations (22)–(24) with $\epsilon = 1$, where we find that in the limit $r \to \infty$, the energy density, as well as the radial and tangential pressures all vanish. This confirms that the wormhole branch $WH+$ is indeed asymptotically flat and describes the exterior regions extending to infinity.

On the other hand, the $WH-$ branch is characterized by the shape function $b_-(r) = \frac{r}{16K(r-r_0)(a-\sqrt{\frac{r-r_0}{K}})+1}$ and describes the intermediate tunnel connecting the throats, valid only for $r_0 \leq r \leq r_0 + Ka^2$. For this branch, the radial component of the metric (21) is given by:

$$g_{rr}^{-} = \frac{16K(r-r_0)\left(a-\sqrt{\frac{r-r_0}{K}}\right)+1}{16K\,(r-r_0)\left(a-\sqrt{\frac{r-r_0}{K}}\right)}. \tag{38}$$

The denominator remains positive in the interval $r_0 \leq r \leq r_0 + Ka^2$, which means that expression (38) changes sign when $r > r_0 + Ka^2$. This indicates that the WH^- branch possesses Lorentzian signature only within the interval $r_0 \leq r \leq r_0 + Ka^2$, thereby restricting this spacetime to this specific range of the radial coordinate. In this case, using the Einstein field equations (22)–(24) with $\epsilon = -1$, we find that at the spherical radius $r = r_0 + Ka^2$ the energy density and pressures of exotic matter are given by

$$\kappa\rho(r_0+Ka^2) = \frac{1+8Ka(r_0+Ka^2)}{(r_0+Ka^2)^2}, \tag{39}$$

$$\kappa p_r(r_0+Ka^2) = -\frac{1}{(r_0+Ka^2)^2}, \tag{40}$$

$$\kappa p_t(r_0+Ka^2) = -\frac{4Ka}{r_0+Ka^2}. \tag{41}$$

It is noteworthy that at this particular radius, the energy density is positive, while both the radial and tangential pressures are negative. This behaviour, which differs from the one exhibited at the throat (see Eqs. (25)–(27)), corresponds to a particular configuration of exotic matter of the geometry, applicable to the WH^- branch.

Now, let us briefly comment on the slope of the shape function $b(r)$ at the throat. From Eq. (17), we find that its first derivative takes the form

$$b'(r) = \frac{-8\sqrt{K}\epsilon\,(r+2r_0)\sqrt{r-r_0} - 16Kar_0 + 1}{\left(16(r-r_0)\left(Ka+\sqrt{K}\epsilon\sqrt{r-r_0}\right)+1\right)^2}. \tag{42}$$

Evaluating this derivative at the throat yields

$$b'(r_0) = 1 - 16Kar_0, \tag{43}$$

which implies that both $b_+(r)$ and $b_-(r)$ possess the same finite slope at r_0. From Eqs. (33) and (34), we conclude that if the wormhole is supported by a positive energy density, then the slope of the shape function at the throat is positive, since in this case $1 - 16Kar_0 > 0$. Conversely, when the energy density is negative, the slope becomes negative as well. In this way, the slope of $b(r)$ at the throats is directly related to the sign of the energy density.

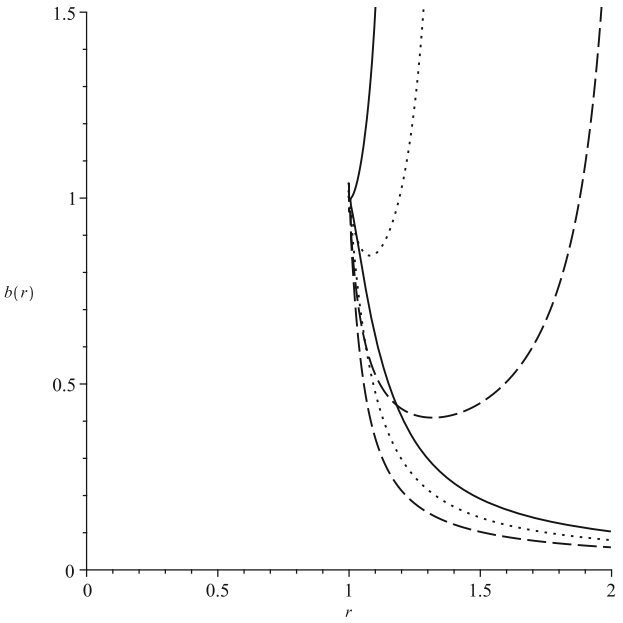

Fig. 2 The figure illustrates the behavior of the composite shape function $b(r)$, given by Eq. (17), for $r_0 = 1$ and $K = 1$, and for three representative values of the parameter a: $a = 0.15$ (solid line), $a = 0.5$ (dotted line), and $a = 1$ (dashed line). Each curve shows both the $b_+(r)$ branch, which extends asymptotically to infinity, and the $b_-(r)$ branch, which describes the intermediate region restricted to $1 \leq r \leq 1 + Ka^2$. All curves meet continuously at the throat location $r = r_0 = 1$ where $b(r_0) = 1$

The composite structure of the solution is illustrated in Fig. 2, where the function $b(r)$ is shown for three representative values of the parameter a: $a = 0.15$ (solid line), $a = 0.5$ (dotted line), and $a = 1$ (dashed line), all for $K = 1$. Each curve displays both the $b_+(r)$ branch extending asymptotically to infinity and the $b_-(r)$ branch covering the intermediate region $r_0 \leq r \leq r_0 + Ka^2$. Notably, larger values of a produce more extended intermediate regions. The continuity at $r = r_0 = 1$, where all curves converge to $b(r_0) = 1$ is evident.

In Fig. 3, we show the behaviour of $b_\pm(r)/r$ for both branches of metric (21). It is evident that both branches satisfy constraint (7) within their respective domains, with $b_+(r)/r \to 0$ as $r \to \infty$ confirming asymptotic flatness.

We now focus on the geometric visualization of the wormhole under consideration. This analysis can be carried out by embedding spacetime slices of the metric (21), defined by $t = const$ and $\theta = \pi/2$, into the three-dimensional Euclidean space. To this end, we make use of Eq. (4).

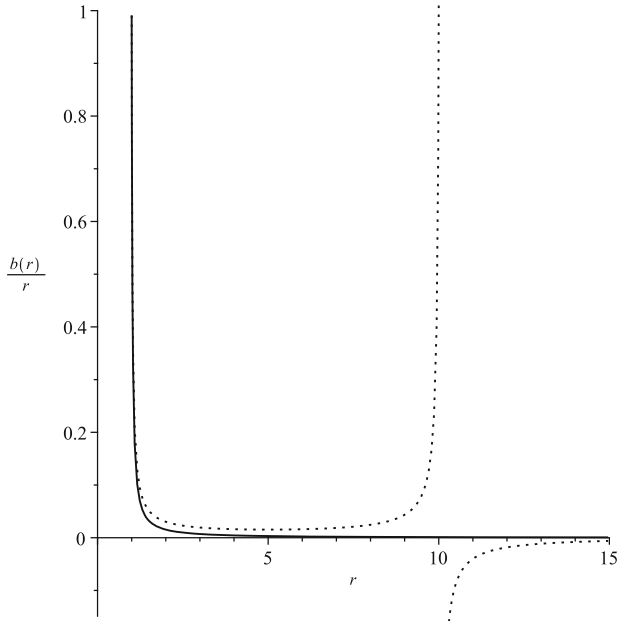

Fig. 3 The figure illustrates the behaviour of $b_{\pm}(r)/r$ for both branches of metric (21) with parameters $a = 3, r_0 = 1$ and $K = 1$. The $b_+(r)$ branch (solid line) satisfies both constraints (6) and (7), where as the $b_-(r)$ branch (dotted line) satisfies only constraint (7)

Due to the method used to construct this family of wormholes, it is evident that substituting the shape function (17) into Eq. (4) leads to Eq. (15) for the lift function $z(r)$, or equivalently, to the set of Eqs. (11)–(14), up to integration constants.

Before analyzing the embedding diagrams of the metric (21) for different values of the parameter a, it is important to note that, for $r = r_0$, Eqs. (11)–(14) show that from the first two equations we obtain $z_1(r_0) = z_2(r_0) = \sqrt{a}$, while from the last two we find $z_3(r_0) = z_4(r_0) = -\sqrt{a}$. Therefore, there exists the continuity between the functions $z_1(r)$ and $z_2(r)$, as well as between $z_3(r)$ and $z_4(r)$, at the throats of the wormhole under study.

On the other hand, it is necessary to verify also the smooth matching between $z_2(r)$ and $z_3(r)$. Since the flare-out condition imposes $a > 0$, it follows that $z_2(r)$ vanishes precisely at $r = r_0 + Ka^2$, while $z_3(r)$ also takes the value zero at the same radius. Therefore, the continuity between $z_2(r)$ and $z_3(r)$ is naturally guaranteed, as both functions smoothly meet at this point of the radial coordinate, ensuring a consistent geometric embedding.

To illustrate the connection structure discussed above, Fig. 4 shows the embedding functions $z_i(r)$ for the parameter values $r_0 = 1$ and $a = 4$. The figure clearly displays how these functions connect: $z_1(r)$ with $z_2(r)$ at the first throat ($r = r_0$), $z_2(r)$ with $z_3(r)$ at the boundary $r = r_0 + Ka^2$, and finally $z_3(r)$ with $z_4(r)$ at the second throat ($r = r_0$). All connections are smooth and continuous, confirming the geometric consistency of the two-throat wormhole configuration.

We now explicitly verify the smoothness of the stress-energy tensor components and the Kretschmann curvature invariant at the two critical radii of the geometry: the shared throat $r = r_0$ and the tunnel boundary $r_* \equiv r_0 + Ka^2$.

At the shared throat $r = r_0$. Both branches of the shape function satisfy $b_{\pm}(r_0) = r_0$ and share the same slope $b'_{\pm}(r_0) = 1 - 16Kar_0$. As explicitly shown in Eqs. (25)–(27), the stress-energy components $\rho(r_0)$, $p_r(r_0)$, and $p_t(r_0)$ are branch-independent: they hold identically for $\varepsilon = +1$ and $\varepsilon = -1$ and for arbitrary $\phi(r)$. This follows from the fact that $(1 - b/r)\big|_{r_0} = 0$, which causes all terms involving ϕ' and ϕ'' to vanish exactly at the throat in the expressions for p_r and p_t. The stress-energy tensor is therefore continuous at $r = r_0$ for any redshift function, with no junction conditions or distributional sources required.

For the Kretschmann curvature invariant $\mathcal{K} \equiv R_{abcd}R^{abcd}$, we use the result for the $\phi = 0$ Morris–Thorne metric,

$$\mathcal{K} = \frac{2(b - b'r)^2 + 4b^2}{r^6}, \tag{44}$$

and substitute $b(r_0) = r_0$ and $b'(r_0) = 1 - 16Kar_0$, obtaining

$$\mathcal{K}(r_0) = \frac{4\left(1 + 128\,K^2a^2r_0^2\right)}{r_0^4}. \tag{45}$$

Since this expression depends only on $b(r_0)$ and $b'(r_0)$, which are identical for both branches, the Kretschmann scalar is continuous at $r = r_0$. The geometry is therefore smooth at the shared throat, with no thin-shell-like behavior.

At the tunnel boundary $r_* = r_0 + Ka^2$, the embedding functions $z_2(r)$ and $z_3(r)$ both vanish, marking the upper boundary of the $\varepsilon = -1$ intermediate tunnel branch. It is important to note that r_* is not a junction between two distinct spacetime patches: both z_2 and z_3 belong to the same $\varepsilon = -1$ branch and therefore share the same shape function $b_-(r)$ and the same stress-energy tensor. The continuity of $T_{\mu\nu}$ at r_* is therefore automatic, as there is a single analytic expression valid throughout the domain $r_0 \le r \le r_*$.

The stress-energy components of the $\varepsilon = -1$ branch at $r = r_*$ are given by Eqs. (39)–(41), and are all finite. The Kretschmann scalar at r_* is obtained by substituting $b_-(r_*) = r_*$ and $b'_-(r_*) = 1 + 8Kar_*$ into Eq. (44), yielding

$$\mathcal{K}(r_*) = \frac{4\left(1 + 32\,K^2a^2r_*^2\right)}{r_*^4}, \tag{46}$$

where $r_* = r_0 + Ka^2$. This is finite, confirming the absence of curvature singularities at the tunnel boundary. Together

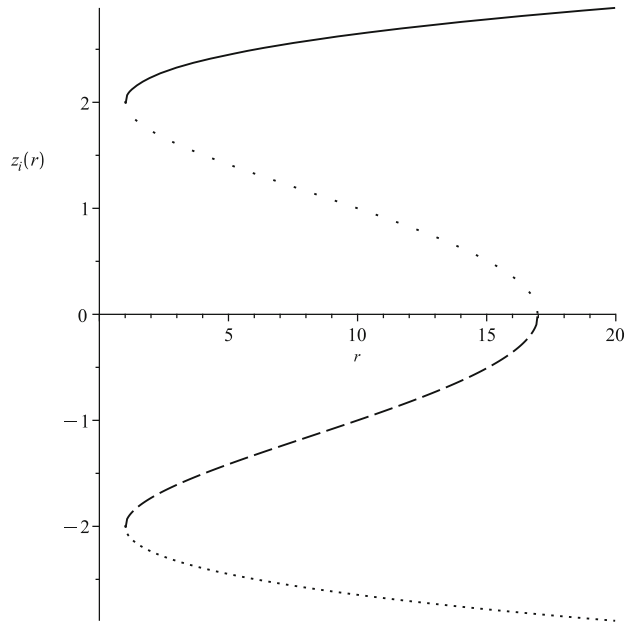

Fig. 4 The figure illustrates the embedding functions $z_i(r)$ for parameter values $K = 1$, $r_0 = 1$ and $a = 4$, demonstrating the smooth and continuous connections discussed previously. The function $z_1(r)$ (solid line) connects with $z_2(r)$ (space-dotted line) at the throat $r = r_0 = 1$ located at $z = +2$. The function $z_2(r)$ then connects with $z_3(r)$ (dashed line) at $r = r_0 + Ka^2 = 17$, where both functions vanish ($z = 0$), defining the radial extension of the intermediate tunnel region. Finally, $z_3(r)$ connects with $z_4(r)$ (dotted line) at the second throat $r = r_0 = 1$ located at $z = -2$. All connections are smooth and continuous, ensuring a well-defined wormhole geometry with two symmetric throats

with the finiteness of the stress-energy components, this rules out any distributional (delta-function) sources at r_*, and no thin-shell junction conditions are needed at any point of the geometry.

It is worth noting an interesting geometric property of the tunnel boundary $r_* = r_0 + Ka^2$. A direct evaluation of the shape function $b_-(r)$ at this radius yields $b_-(r_*) = r_*$, which formally resembles the throat condition (2). However, this does not imply that r_* is a wormhole throat. A genuine throat requires, in addition to $b(r_{\rm th}) = r_{\rm th}$, that the flare-out condition be satisfied, i.e., $b'(r_{\rm th}) < 1$, which guarantees that $r_{\rm th}$ is a *minimum* of the radial coordinate $r(z)$ along the embedding. Evaluating the derivative of $b_-(r)$ at r_* gives

$$b'_-(r_*) = 1 + 8Ka\left(r_0 + Ka^2\right) = 1 + 8Ka\, r_* > 1, \qquad (47)$$

which strictly violates the flare-out condition for all $a, K, r_0 > 0$. Equivalently, the quantity governing the second derivative of r with respect to z satisfies

$$b_-(r_*) - r_*\, b'_-(r_*) = -8Ka\left(r_0 + Ka^2\right)^2 < 0, \qquad (48)$$

so that $d^2r/dz^2 < 0$ at r_*. This means that r_* is a *maximum* of $r(z)$, not a minimum: it corresponds to the widest circle of the intermediate tunnel, i.e., an anti-throat or *equator* of the geometry. This is precisely the behavior visible in the three-dimensional embedding diagrams of Figs. 4 and 5, where r_* marks the maximum radius of the tunnel connecting the two throats at r_0.

Having established the continuity of the embedding functions, we now proceed to analyze the first configuration, which corresponds to a wormhole sustained by an exotic fluid characterized by a negative energy density. According to Eq. (34), achieving $\rho(r_0) < 0$ at the throat requires that the parameters involved satisfy the condition $a > \frac{1}{16Kr_0}$. When this inequality is satisfied, all radicands in the functions $z_i(r)$ appearing in Eqs. (11)–(14) remain positive for $r > r_0$, which implies that the embeddings are well-defined over the entire wormhole. This situation is illustrated in Fig. 5.

The figure clearly illustrates the presence of two symmetric throats in the wormhole geometry, in contrast with the standard embedding diagram, which exhibits a single throat. Near each throat, the curves display symmetric singular behaviors with abrupt changes in slope. Such a double-throat structure reflects a more intricate geometry than the classical Morris–Thorne configuration, where the energy conditions are violated at both throats. The parameter a plays a crucial role in determining the sharpness of the throat geometry: larger values of a produce more pronounced and sharply defined throats, as evidenced by the steeper slopes of the embedding functions near $r = r_0$, while smaller values of a yield smoother, more gradual throat structures. At large radial distances, the embedding functions converge asymptotically, indicating that the geometry approaches a flat spacetime configuration. This asymptotic behavior confirms that the wormhole solutions satisfy the requirement of asymptotic flatness, with the exotic matter effects becoming negligible far from the throat regions.

To provide a more intuitive visualization of the wormhole geometry, Fig. 6 presents the three-dimensional embedding diagram for $a = 2$, obtained by rotating the corresponding profile from Fig. 5 around the symmetry axis. The resulting surface clearly displays the two-throat structure: the narrow constrictions at $r = r_0$ correspond to the two throats connecting the asymptotically flat exterior regions with the intermediate tunnel, while the wide circle at $r_1 = r_0 + Ka^2$ marks the maximum radius of the tunnel where the upper and lower branches of the $\varepsilon = -1$ solution meet at $z = 0$.

We now turn to the configuration corresponding to a wormhole sustained by an exotic fluid with positive energy density. From Eq. (33), it follows that, in order to ensure $\rho(r_0) > 0$ at the throat, the parameters must satisfy the inequality $0 < a < \frac{1}{16Kr_0}$. Under this condition, all the embedding functions $z_i(r)$ defined in Eqs. (11)–(14) remain positive for $r > r_0$, indicating that the wormhole possesses

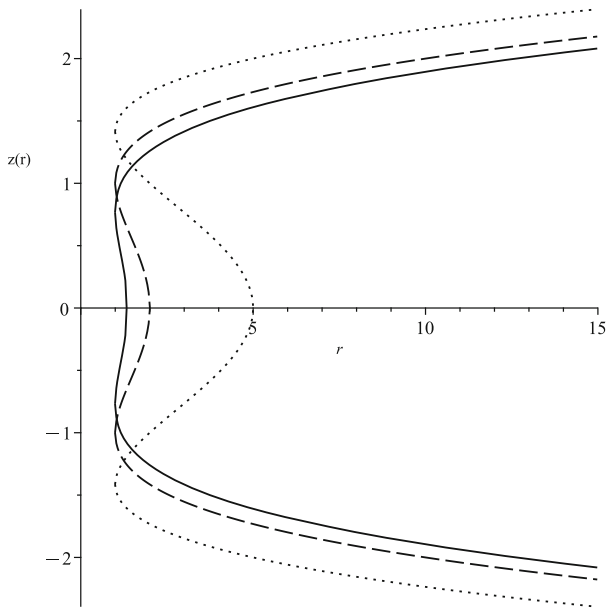

Fig. 5 The figure shows the embedding diagrams of metric (21) for $t = \text{const}$, $\theta = \pi/2$, $K = 1$ and $r_0 = 1$. The plots correspond to a wormhole sustained by negative energy density, with parameter values $a = 0.5$ (solid line), $a = 1$ (dashed line), and $a = 2$ (dotted line)

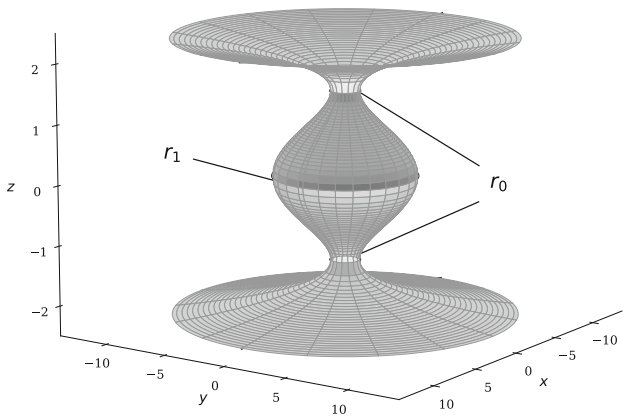

Fig. 6 Three-dimensional embedding diagram of the two-throat wormhole for $K = 1$, $a = 2$ and $r_0 = 1$, constructed from the embedding functions (11)–(14). Two asymptotically flat exterior regions (upper and lower sheets) are connected by an intermediate tunnel. The narrow circles at r_0 indicate the throats, while the wide circle at $r_1 = r_0 + Ka^2$ (in this figure with $K = 1$) corresponds to the maximum radius of the tunnel, where the z_2 and z_3 branches meet at $z = 0$

two throats. These throats are considerably less pronounced than those found in the previous case with negative energy density, as shown in Fig. 7. This contrast in the sharpness of the throat geometry highlights the different behaviors of the energy conditions in configurations with positive and negative energy densities.

To provide a more intuitive visualization of the wormhole geometry in the case of positive energy density $\rho(r_0) > 0$, Fig. 8 displays the corresponding three–dimensional embedding for $K = 1$ and $a = 0.0624$. In comparison with Fig. 6, the tunnel region is dramatically compressed: whereas for $a = 2$ the tunnel extends over a radial interval $\Delta r = Ka^2 = 4$, for $a = 0.0624$ it spans only $\Delta r \approx 4 \times 10^{-3}$. This behavior clarifies why configurations satisfying $\rho(r_0) > 0$ require extremely small values of a: the two throats become nearly coincident, and the geometry approaches the limiting configuration of a single–throat wormhole.

A noteworthy feature of the positive energy density configurations is that they necessarily correspond to extremely small values of the parameter a, specifically $0 < a < 1/(16Kr_0)$. Since the tunnel length scales as $\Delta r = Ka^2$ and the vertical throat separation as $\Delta z = 2\sqrt{a}$, these constraints imply that wormholes supported by phantom matter possess an almost imperceptible intermediate region, with $r_1 \approx r_0$. In this regime, the two throats become nearly coincident and the geometry closely resembles that of a single-throat wormhole. This behavior is clearly illustrated in Fig. 7, where for $a = 0.0624$ the tunnel extends over a radial interval of only $\Delta r \approx 0.004$. Thus, while it is formally possible to construct two-throat wormholes sustained by phantom matter ($\rho > 0$, $\omega_r < -1$), the geometric distinction between the two throats becomes practically undetectable, and the configuration approaches the limiting case of the standard Morris-Thorne single-throat geometry.

A comparison between both families of solutions reveals three key distinctions. First, concerning the parameter space: configurations with negative energy density allow greater freedom ($a > \frac{1}{16Kr_0}$), whereas those with positive energy density are restricted to the narrow range $0 < a < \frac{1}{16Kr_0}$. Second, regarding the violation of the energy conditions: the $\rho < 0$ family exhibits stronger violations of the NEC and WEC, accompanied by steeper slopes near the throat, while $\rho > 0$ configurations display milder departures from the standard energy conditions. Third, in terms of geometry: the $\rho < 0$ solutions develop sharp, well-defined throats, whereas $\rho > 0$ cases exhibit smoother and more gradual throat structures, associated with a less extreme curvature of the embedding surface.

The role of the parameter a extends beyond the matter content and geometric structure discussed above: it also governs how the gravitational influence of the wormhole is distributed in space. For an asymptotically flat Morris–Thorne wormhole with $\phi = 0$, the ADM mass is determined by the asymptotic behavior of the shape function via $M_{\text{ADM}} = \lim_{r\to\infty} b_+(r)/2$ [15]. Expanding $b_+(r)$ for large r, one finds

$$b_+(r) = \frac{1}{16\sqrt{K}}\, r^{-1/2} + \mathcal{O}(r^{-1}), \qquad r \to \infty, \tag{49}$$

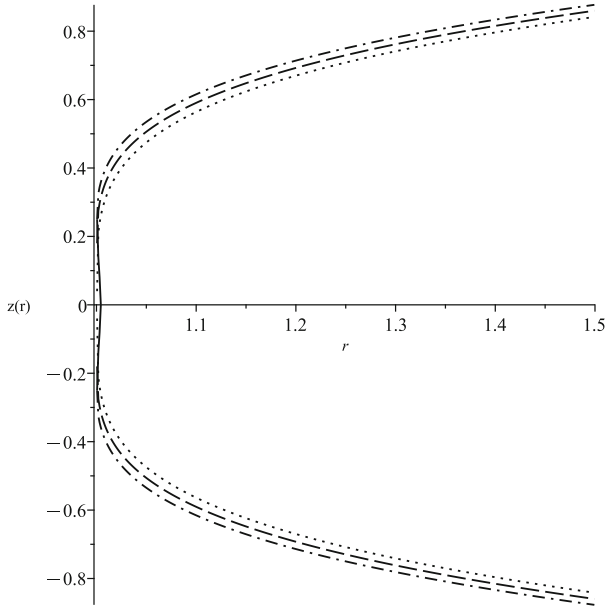

Fig. 7 The figure presents the embedding diagrams of metric (21) for $t = \text{const}$, $\theta = \pi/2$, $K = 1$ and $r_0 = 1$. The curves illustrate a wormhole supported by positive energy density, plotted for $a = 0.00159$ (dotted line), $a = 0.0324$ (dashed line), and $a = 0.0624$ (dash-dotted line)

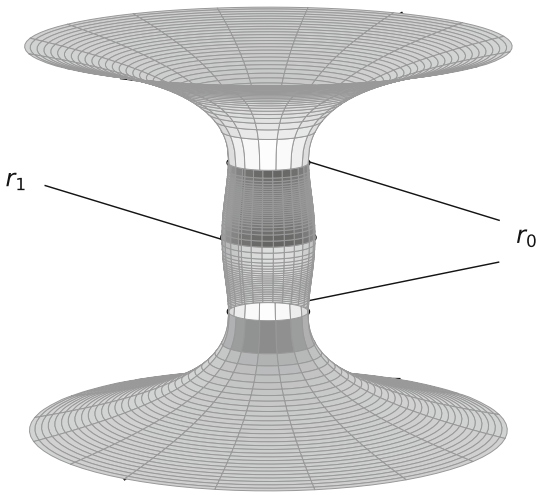

Fig. 8 Three-dimensional embedding diagram for $K = 1, a = 0.0624$ and $r_0 = 1$. To better visualize the two-throat structure, both the vertical scale and the tunnel width have been exaggerated. The narrow circles at r_0 indicate the two throats, while the wider circle at $r_1 = r_0 + Ka^2$ (in this figure with $K = 1$) marks the maximum radius of the intermediate tunnel. In contrast to the case $a = 2$ shown in Fig. 6, where the tunnel exhibits a pronounced hourglass shape, here the two throats at r_0 are much closer together since the tunnel length scales as $Ka^2 \approx 0.004$

so that $b_+(r) \to 0$ as $r \to \infty$, and therefore

$$M_{\text{ADM}} = \lim_{r\to\infty} \frac{b_+(r)}{2} = 0. \tag{50}$$

The ADM mass vanishes for all values of the throat-separation parameter a. Unlike the Schwarzschild spacetime, where $b = r_s = \text{const}$ yields $M_{\text{ADM}} = r_s/2 \neq 0$, here $b_+(r) \to 0$ as $r \to \infty$, so the wormhole carries no net gravitational mass as measured by a distant observer. The influence of a on the gravitational field is instead encoded in the local effective mass $M_{\text{eff}}(r) = b_+(r)/2$. At the throat, $M_{\text{eff}}(r_0) = r_0/2$ independently of a. For $r > r_0$, one has $\partial b_+/\partial a < 0$, so that larger values of a produce smaller values of $M_{\text{eff}}(r)$ at every fixed radius outside the throat. Thus, increasing the throat separation concentrates the gravitational influence of the wormhole closer to the throat, while the total ADM mass remains zero throughout the entire family of solutions.

To summarize the constraints discussed above, Fig. 9 presents the complete parameter space analysis for both branches. For the $\varepsilon = +1$ branch (left panel), the flare-out condition (19) is automatically satisfied for all $a > 0$, leaving the energy density sign as the only physical distinction: configurations with $a < a_c$ yield $\rho(r_0) > 0$ (hatched region), while $a > a_c$ corresponds to $\rho(r_0) < 0$ (gray region). The $\varepsilon = -1$ branch (right panel) exhibits a more constrained parameter space. The geometric restriction (38) limits the valid domain to $r \leq r_0 + Ka^2$ (region to the left of the solid curve), while the flare-out condition (19) requires $a > \frac{3}{2\sqrt{K}}\sqrt{r - r_0}$ (region above the dashed curve). The intersection of these constraints defines the physically viable configurations: the light gray region satisfies all conditions with $\rho(r_0) < 0$, whereas positive energy density (hatched region) is restricted to an extremely narrow strip near $r = r_0$, requiring both $a < a_c$ and $a > \frac{3}{2\sqrt{K}}\sqrt{r - r_0}$ simultaneously.

To summarize the geometric properties of the two-throat wormhole, Fig. 10 displays the vertical separation between the throats, $\Delta z = 2\sqrt{a}$, and the tunnel length, $\Delta r = Ka^2$, as functions of the parameter a. Both quantities increase monotonically with a: for $K = 1$ and small values such as $a = 0.0624$ (corresponding to $\rho(r_0) > 0$), the throats are nearly coincident, while for larger values such as $a = 2$, the two-throat structure becomes clearly distinguishable, as illustrated in the embedding diagrams of Figs. 6 and 8.

5 Conclusions

While the standard Morris-Thorne wormhole geometry features a single throat connecting two asymptotically flat regions, the possibility of multi-throat configurations represents a natural generalization that deserves systematic exploration. From a theoretical perspective, wormholes with multiple throats offer several advantages and insights compared to their single-throat counterparts. First, they provide a richer geometric structure that allows for the study of intermedi-

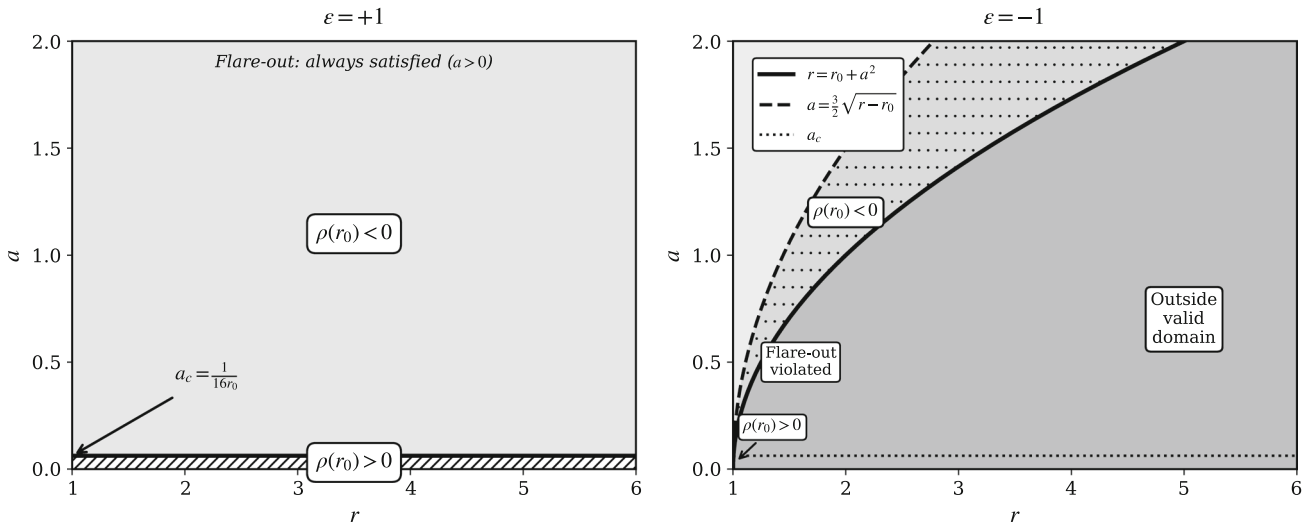

Fig. 9 Parameter space for the two-throat wormhole with $K = 1$ and $r_0 = 1$. **Left panel** ($\varepsilon = +1$): the flare-out condition is satisfied for all $a > 0$. The diagonal hatched region ($0 < a < a_c$) has $\rho(r_0) > 0$, while the gray region ($a > a_c$) has $\rho(r_0) < 0$. **Right panel** ($\varepsilon = -1$): the dark gray region lies outside the valid domain ($r > r_0 + Ka^2$). The dotted region, located below the dashed curve $a = \frac{3}{2\sqrt{K}}\sqrt{r - r_0}$ and to the left of the solid curve $r = r_0 + Ka^2$, violates the flare-out condition. The light gray region, located above the dashed curve and to the left of the solid curve, satisfies both the domain and flare-out conditions with $\rho(r_0) < 0$. The narrow diagonal hatched region near $r = r_0$ also satisfies all geometric constraints but with $\rho(r_0) > 0$; for $K = 1$ this region is extremely small since it requires simultaneously $a < a_c = 1/(16Kr_0)$ and $a > \frac{3}{2\sqrt{K}}\sqrt{r - r_0}$

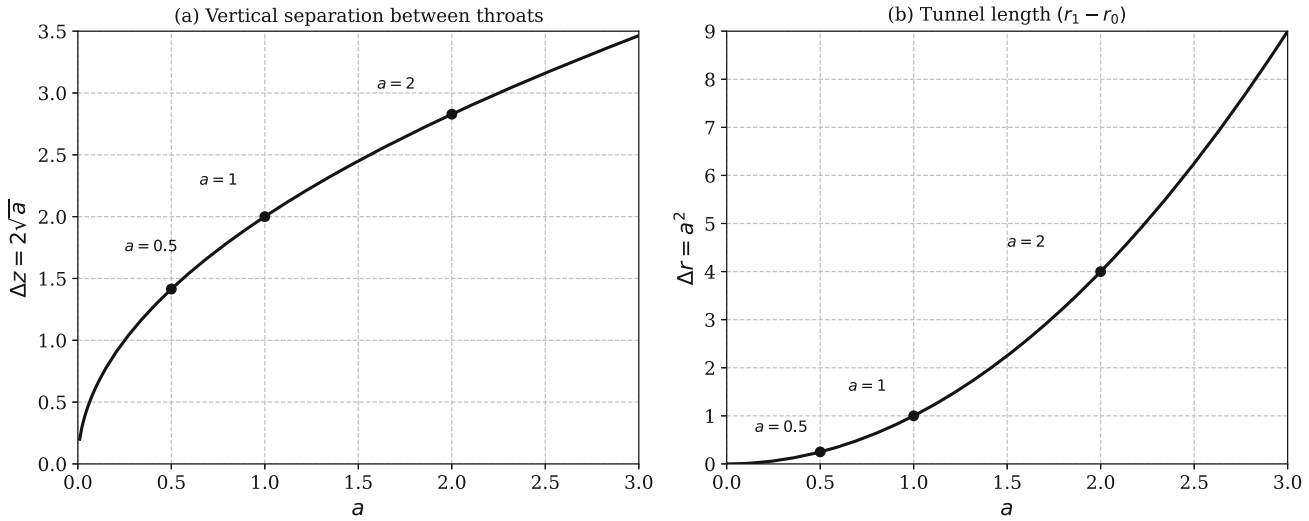

Fig. 10 Geometric properties of the two-throat wormhole as a function of the parameter a for $K = 1$ and $r_0 = 1$. (a) Vertical separation between the throats in the embedding space, $\Delta z = 2\sqrt{a}$, obtained from Eq. (20). (b) Tunnel length in the radial coordinate, $\Delta r = r_1 - r_0 = Ka^2$, derived from Eq. (18). The marked values $a = 0.5$, 1, and 2 correspond to the embedding diagrams presented in Fig. 5 for negative energy density configurations, while smaller values correspond to the positive energy density cases shown in Fig. 7. Both quantities vanish as $a \to 0$, corresponding to the limiting case where the two throats merge into a single-throat configuration

ate tunnel regions with restricted radial domains, which may lead to different distributions of exotic matter and potentially novel violations of energy conditions. Second, multi-throat geometries introduce additional geometric parameters, such as the throat separation and the size of the intermediate regions, that can be adjusted to investigate how the amount and distribution of exotic matter scale with the underlying geometric complexity. Third, such configurations may

offer new mechanisms for minimizing the total amount of exotic matter required to sustain the wormhole, as the matter could be distributed across multiple throats rather than concentrated at a single junction. Finally, from an astrophysical standpoint, multi-throat wormholes could exhibit distinct observational signatures in gravitational lensing or accretion dynamics compared to single-throat geometries, providing potential avenues for observational discrimination.

In this work, we have successfully constructed a family of traversable Lorentzian wormholes with two symmetric throats, using a geometric approach based on analytic embedding functions. Our methodology is grounded in the embedding condition obtained by embedding spacelike slices of the Morris–Thorne metric into Euclidean space, which ensures that the flare-out condition, essential for traversable wormhole geometries, is satisfied.

The key contribution of our approach lies in the systematic construction of multi-throat wormhole configurations using the ansatz (9) for the embedding function. This choice yields a well-defined shape function (17) that satisfies all geometric constraints for traversable wormholes, including the throat condition (2), the flare-out condition, and asymptotic flatness. The resulting geometry exhibits two symmetric throats located at $z = \pm\sqrt{a}$ in the embedding space, with a throat separation of $2\sqrt{a}$, connected through an intermediate region where each throat independently satisfies the necessary geometric conditions.

A crucial structural feature of our solution is its composite nature, consisting of two distinct branches characterized by the parameter $\epsilon = \pm 1$. The $\epsilon = +1$ branch describes the asymptotically flat exterior regions extending from each throat to spatial infinity, where all components of the energy–momentum tensor vanish as $r \to \infty$. In contrast, the $\epsilon = -1$ branch represents the intermediate tunnel connecting the two throats, with a restricted geometric domain $r_0 \leq r \leq r_0 + Ka^2$. This restricted domain emerges naturally from the requirement that the metric maintain Lorentzian signature, as the radial metric component g_{rr}^{-} changes sign for $r > r_0 + Ka^2$. The continuity and smooth matching of the embedding functions $z_i(r)$ at both the throats ($r = r_0$) and the tunnel boundary ($r = r_0 + Ka^2$) ensure a geometrically consistent configuration, as evidenced by Fig. 4.

Our analysis of the Einstein field equations reveals that the exotic matter supporting this two-throat configuration necessarily violates classical energy conditions. Specifically, the WEC, NEC, and DEC are systematically violated throughout the spacetime, while the SEC is exactly satisfied with $\rho + p_r + 2p_t = 0$. This violation pattern is consistent with the fundamental requirement that traversable wormholes must be sustained by exotic matter.

A key result reveals a clear link between the geometric scale of the wormhole and the properties of its matter content. The parameter a, which controls the throat separation $2\sqrt{a}$, also determines the sign and magnitude of the energy density at the throats through the critical value $a_c = \frac{1}{16Kr_0}$. For configurations with $0 < a < \frac{1}{16Kr_0}$, corresponding to closely spaced throats, the energy density remains positive ($\rho(r_0) > 0$) while the matter exhibits phantom-type behavior characterized by a radial equation of state parameter $\omega_r < -1$ and an effective equation of state $\omega_{\text{eff}} < 0$, indicating dark-energy-like behavior on average. Conversely, for $a > \frac{1}{16Kr_0}$, representing more widely separated throats, the configuration requires negative energy density ($\rho(r_0) < 0$). This relationship suggests that reducing the throat separation in multi-throat wormholes favors configurations with weaker violations of the classical energy conditions, since positive energy density combined with phantom-type pressure is physically less exotic than negative energy density.

The geometric visualization through embedding diagrams (Figs. 5, 7) reveals a striking qualitative difference between these two regimes. Configurations with negative energy density ($a > \frac{1}{16Kr_0}$) feature well-defined throats and steep slopes in their embedding functions, reflecting stronger curvature and more pronounced geometric features. In contrast, positive energy density configurations ($0 < a < \frac{1}{16Kr_0}$) display smoother, more gradual throat structures with less extreme curvature. This geometric distinction provides a visual manifestation of the different energy condition violations in each regime. Furthermore, the parameter a controls not only the throat separation but also the sharpness of the throat geometry: Larger values produce more pronounced throats with steeper embedding function slopes near $r = r_0$, while smaller values yield smoother, more gradual structures.

The geometric construction presented in this work demonstrates that multi-throat wormhole configurations can be systematically generated through embedding techniques, offering new insights into exotic spacetime topologies within the framework of General Relativity. Recent field-theoretic approaches have reached related but distinct results. Rodrigues and Silva [7,13] constructed black-bounce spacetimes with multiple throats and anti-throats by postulating a metric function $\Sigma(r)$ and deriving phantom scalar field and NED sources from the Einstein equations; in their approach, multi-throat structure is identified *a posteriori* through extrema of the areal function, and the solutions include configurations with horizons, differing from the purely traversable geometries studied here. Crispim et al. [8] further analyzed the same class of geometries, showing that distinct scalar field profiles generate identical spacetime structures, and that energy conditions can be partially satisfied in localized regions for appropriate parameter choices. Chew and Lim [16,17] obtained double-throat configurations in Einstein–Yang–Mills–Higgs theory, while Emparan et al. [18] constructed multi-mouth wormholes by inserting black holes into existing throat geometries, and Bron-

nikov and Skvortsova [19] investigated axially symmetric multi-wormhole solutions. In contrast, the present approach derives the two-throat geometry directly from the embedding ansatz (9), with the flare-out condition satisfied by construction at both throats and traversability guaranteed throughout the entire parameter space. The throat separation $2\sqrt{a}$ enters as an explicit geometric parameter that governs analytically the sign of the energy density at the throats through the critical value $a_c = \frac{1}{16Kr_0}$, a direct link between topological scale and matter exoticity without counterpart in the field-theoretic constructions cited above.

This work presents one of the first systematic studies of asymptotically flat traversable wormholes with two symmetric throats within the Morris–Thorne framework, addressing a configuration that has received comparatively little attention despite its natural role as the simplest non-trivial extension of standard single-throat geometries. The key methodological contribution is the embedding ansatz (9), which guarantees by construction the presence of exactly two throats satisfying the flare-out condition throughout the entire parameter space, without requiring a specific field-theoretic source. Several promising observational and phenomenological directions emerge naturally from this foundation. The closed-form shape function (17) provides the complete analytical input required to study null geodesics and the effective potential for photon motion, enabling the computation of deflection angles and gravitational lensing profiles. The shadow morphology as seen by a distant observer and the accretion dynamics around this object, following the approach of Ref. [14], represent further natural extensions [7,8]. Finally, the generalization to more than two throats could be systematically explored by extending the ansatz to higher-order polynomial forms, potentially revealing how matter requirements and observational signatures scale with topological complexity.

Acknowledgements This work was supported by the Dirección de Investigación y Creación Artística at the Universidad del Bío-Bío through grants No. RE2320220 (MC), GI2310339 (AC, MC and PL) and RE2320212 (PL).

Data Availability Statement This manuscript has no associated data. [Authors' comment: Data sharing not applicable to this article as no datasets were generated or analysed during the current study.].

Code Availability Statement The manuscript has no associated code/software. [Author's comment: Maple and Python were used for symbolic computation and numerical analysis during the study. The code is not publicly available.].

Funded by SCOAP[3].

References

1. M.S. Morris, K.S. Thorne, Wormholes in spacetime and their use for interstellar travel: a tool for teaching general relativity. Am. J. Phys. **56**, 395 (1988)
2. M.S. Morris, K.S. Thorne, U. Yurtsever, Wormholes, time machines, and the weak energy condition. Phys. Rev. Lett. **61**, 1446 (1988)
3. J.P.S. Lemos, F.S.N. Lobo, Plane symmetric traversable wormholes in an anti-de Sitter background. Phys. Rev. D **69**, 104007 (2004)
4. C. Barcelo, L.J. Garay, P.F. Gonzalez-Diaz, G.A. Mena Marugan, Asymptotically anti-de Sitter wormholes. Phys. Rev. D **53**, 3162 (1996)
5. J.P.S. Lemos, F.S.N. Lobo, S.Q. de Oliveira, Morris–Thorne wormholes with a cosmological constant. Phys. Rev. D **68**, 064004 (2003)
6. M. Visser, *Lorentzian Wormholes: From Einstein to Hawking* (American Institute of Physics, New York, 1995)
7. M.E. Rodrigues, M.V. de S. Silva, Black-bounces with multiple throats and anti-throats. Class. Quantum Gravity **40**, 225011 (2023)
8. T.M. Crispim, M.V. de S. Silva, G. Alencar, C.R. Muniz, D. Sáez-Chillón Gómez, Field sources for wormholes with multiple throats/anti-throats. Class. Quantum Gravity **42**, 085005 (2025)
9. R.R. Caldwell, A phantom menace? Cosmological consequences of a dark energy component with super-negative equation of state. Phys. Lett. B **545**, 23 (2002)
10. R.R. Caldwell, M. Kamionkowski, N.N. Weinberg, Phantom energy: dark energy with $w < -1$ causes a cosmic doomsday. Phys. Rev. Lett. **91**, 071301 (2003)
11. F.S.N. Lobo, Phantom energy traversable wormholes. Phys. Rev. D **71**, 084011 (2005)
12. A. Rueda, R. Avalos, E. Contreras, Construction of a traversable wormhole from a suitable embedding function. Eur. Phys. J. C **82**, 605 (2022)
13. M.E. Rodrigues, M.V. de S. Silva, Spherically symmetric and static black bounces with multiple horizons, throats, and anti-throats in four dimensions. Class. Quantum Gravity **42**, 055005 (2025)
14. A. Rueda, E. Contreras, Geodesic analysis and steady accretion on a traversable wormhole. Ann. Phys. **459**, 169540 (2023)
15. R. Arnowitt, S. Deser, C.W. Misner, The dynamics of general relativity, in *Gravitation: An Introduction to Current Research*, ed. L. Witten (Wiley, New York, 1962), pp. 227–265; reprinted as arXiv:gr-qc/0405109
16. X.Y. Chew, K.-G. Lim, Non-Abelian wormholes threaded by a Yang-Mills-Higgs field in the BPS limit. Phys. Rev. D **102**, 124068 (2020)
17. X.Y. Chew, K.-G. Lim, Non-Abelian wormholes threaded by a Yang-Mills-Higgs field beyond the BPS limit. Phys. Rev. D **105**, 084058 (2022)
18. R. Emparan, B. Grado-White, D. Marolf, M. Tomaševic, Multi-mouth traversable wormholes. JHEP **05**, 032 (2021)
19. K.A. Bronnikov, M.V. Skvortsova, Cylindrically and axially symmetric wormholes. Throats in vacuum? Gravit. Cosmol. **20**, 171 (2014)